optica

Full optical characterization of single nanoparticles using quantitative phase imaging: supplementary material

SAMIRA KHADIR[1,*], DANIEL ANDRÉN[2], PATRICK C. CHAUMET[1], SERGE MONNERET[1], NICOLAS BONOD[1], MIKAEL KÄLL[2], ANNE SENTENAC[1], AND GUILLAUME BAFFOU[1,**]

[1] *Institut Fresnel, CNRS, Aix Marseille Univ, Centrale Marseille, Marseille, France*
[2] *Department of Physics, Chalmers University of Technology, 412 96 Göteborg, Sweden*
[*] *e-mail: samira.khadir@fresnel.fr*
[**] *e-mail: guillaume.baffou@fresnel.fr*

Published 17 March 2020

This document provides supplementary information to "Full optical characterization of single nanoparticles using quantitative phase imaging," https://doi.org/10.1364/OPTICA.381729.

1. EXPERIMENTAL SETUP

Quadriwave lateral shearing interferometry (QLSI) is an optical technique capable of mapping in a single interferogram acquisition not only the intensity but also the phase gradient of a given light beam in two dimensions.

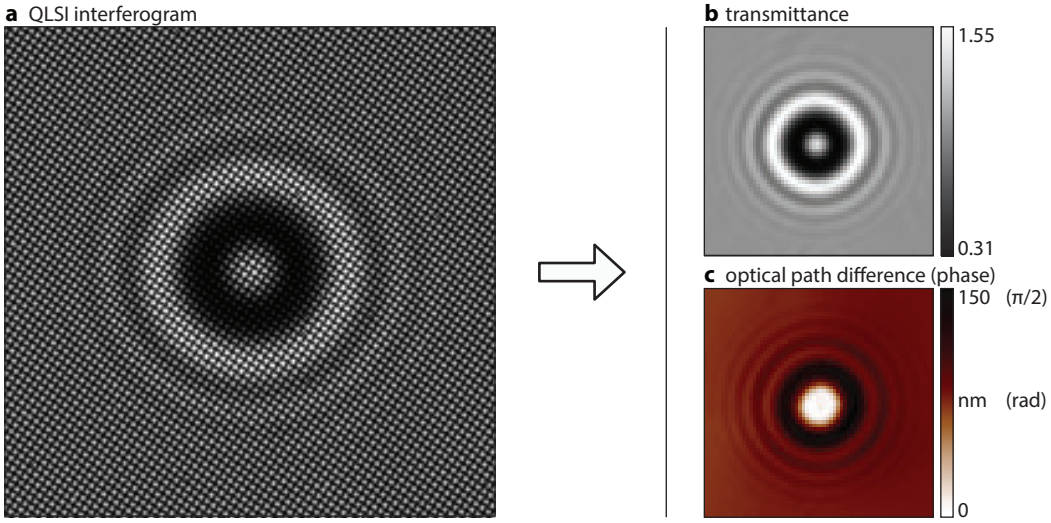

Fig. S1. (a) Raw camera image, called the interferogram, of a 2-µm polystyrene bead in water on glass obtained in a QLSI measurement. Transmittance (b) and optical path density (phase) (c) extracted from the interferogram.

Mapping the phase of a light beam amounts to mapping the profile of the wavefront of the light beam, or equivalently the optical path difference (OPD) created by the object in the field of view of the microscope [1–3]. QLSI is simply based on the use of a specific camera that consists of a two-dimensional (2D) grating (usually called a modified Hartmann mask, MHM) mounted at a millimetric distance from a regular camera [4] (Sid4sC8 Phasics S.A. in this study). Due to the 2D-grating, the image is replicated in four identical but slightly shifted copies, interfering with each other, yielding the formation of an interferogram on the camera sensor. The interferogram is numerically processed in real time using a commercial algorithm (Phasics S.A.) to retrieve both the intensity and the wavefront profiles of the incoming light [5]. To perform measurements on particles, the QLSI camera is plugged into an optical microscope (home made microscope in our case) as shown on Fig. S2. A Köhler configuration was used to illuminate the sample with a controlled optical beam (controlled illuminated area and numerical aperture). 17 different LEDs (from Thorlabs) of different colors

were used to vary the illumination wavelength and carry out the spectral measurements (405, 420, 430, 455, 470, 505, 530, 565, 590, 617, 625, 665, 680, 700, 730, 780, 850 nm). Note that interferences do occur on the camera sensor even if the illumination does not involve a laser. The Köhler configuration ensures a sufficient spatial coherence on the sample plane even with a non-coherent source, and enables the adjustment of both the illuminated area and, more importantly for this study, the numerical aperture (NA) of illumination. When opening the illumination NA, one reduces the spatial coherence of the light at the sample plane. But this does not affect the quantitative nature of the measurements using QLSI. The effects of increasing the NA are (i) an increase of illumination intensity, (ii) an improvement of the spatial resolution of the image and (iii) an optical sectioning of the imaged object in z. This has been discussed by our group in 2014 in the context of living cell imaging [6]. In the context of nanoparticle imaging, there is no relevant z-sectioning effect since the objects are already highly localized in z. The only relevant effect concerns the physics: for some system geometries, the optical cross section may depend on the incidence angle of the light. Opening the numerical aperture of the illumination would then average the optical properties over a given range of illumination. However, the NA of the condenser of a typical Köhler illumination remains small, typically below 0.4 (23°). Thus, we don't expect too strong an effect.

Note that sources with long temporal coherence (lasers) are detrimental as they yield fringes or speckle on the intensity and phase images. Their amplitudes is weak, but when working on nanoparticles also characterized by a weak signal, they can preclude any quantitative measurement. For instance, using a supercontinuum for spectroscopy measurements is not advised for this reason.

Other quantitative phase imaging techniques exist, which could also map the intensity and phase of the light, but QLSI is the only one that provides high-spatial resolution (diffraction limited), high sensitivity (below 1 nm·Hz$^{-1/2}$ in OPD) and quantitative measurements, important requirements for measurements on small particles.

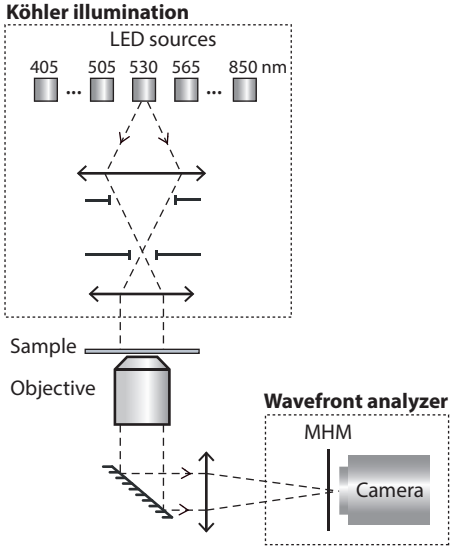

Fig. S2. Scheme of a QLSI microscope setup. A LED based Köhler illumination is used to illuminate the sample with a light beam controlled in size and numerical aperture. A series of LEDs mounted on a carrousel is used to illuminate the particles of the sample at different wavelengths, over the visible-nearIR range.

2. DESCRIPTION OF THE THEORETICAL MODEL ALLOWING TO RETRIEVE THE COMPLEX POLARIZABILITY α

A. Derivation of the expression of α involving image integration

In this section, we detail the underlying theory of PIWI (processing the intensity and wavefront images) to retrieve the complex polarizability of a single nanoparticle in a homogenous medium. We consider the complex dipolar polarizability α of a nanoparticle localized in $\mathbf{r}_0 = (x_0, y_0, z_0)$ defined by

$$\alpha = \frac{1}{\varepsilon_0 |\mathbf{E}_{\text{inc}}(\mathbf{r}_0)|^2} \mathbf{E}^{\star}_{\text{inc}}(\mathbf{r}_0) \cdot \mathbf{p}. \tag{S1}$$

where $\mathbf{p}$ is the complex electric dipole moment of the nanoparticle and $\mathbf{E}_{\text{ex}}$ the local complex electric field. In the following, we will consider a plane wave at normal incidence defined by

$$\mathbf{E}_{\text{inc}}(\mathbf{r}) \hat{=} \mathbf{E}_{\text{ex,ob}}(\mathbf{r}) = \mathbf{E}_0 e^{in\mathbf{k}_0 \cdot \mathbf{r}} = \mathbf{E}_0 e^{ink_0 z}, \tag{S2}$$

where $\mathbf{k}_0 = (0, 0, k_0)$. All the complex quantities refer to physical quantities oscillating at ω, the angular frequency of the incoming light.

In order to retrieve the complex polarizability from the transmission images obtained by QLSI (Eq. (4) of the main manuscript), one needs first to quantitatively model the image of the nanoparticle, in intensity and phase, through an optical microscope. A scheme of the considered system is shown in Fig. S3. The nanoparticle is placed in a homogenous medium represented by its refractive index n. (Oz) is the optical axis of the microscope. The object plane of the microscope corresponds to $z = z_{\text{ob}}$. The nanoparticle is placed at the origin $\mathbf{r}_0 = (0, 0, 0)$. Thus,

$$\mathbf{E}_{\text{ex,ob}}(\mathbf{r}_0) = \mathbf{E}_0. \tag{S3}$$

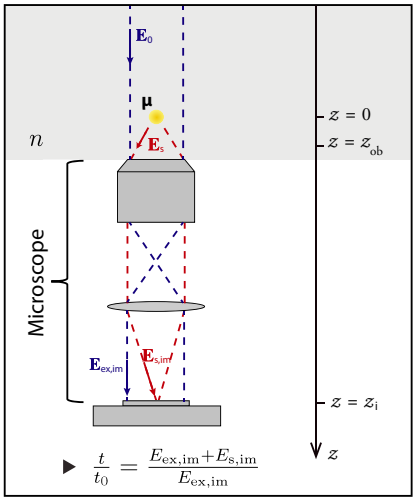

Fig. S3. Description of the model used to retrieve the complex polarizability of a nanoparticle from its response through an optical microscope.

In the absence of nanoparticle, the electric field at the image plane of the microscope with a magnification M is uniform and reads [**?**]:

$$\mathbf{E}_{\text{ex,im}}(\mathbf{r}_{\parallel}) = \mathbf{E}_{\text{ex,im}} = \frac{1}{M}\sqrt{n}\mathbf{E}_0 e^{ink_0 z_{\text{ob}}}, \tag{S4}$$

where $\mathbf{r}_{\parallel} = (x_{\text{im}}, y_{\text{im}})$. In the presence of the nanoparticle, the total electric field at the image plane is given by the sum of the excitation field and the field scattered by the nanoparticle $\mathbf{E}_{\text{tot,im}} = \mathbf{E}_{\text{ex,im}} + \mathbf{E}_{\text{s,im}}$. The analytical expression of the scattered field by an oscillating dipole at the image plane has been demonstrated in our previous work [**?**], it reads:

$$\mathbf{E}_{\text{s,im}}\left(\mathbf{r}_{\parallel}\right) = M \iint_{\text{N.A.}} \sqrt{\frac{\gamma}{\gamma'}} h(M\mathbf{k}'_{\parallel}) \mathbf{e}'(M\mathbf{k}'_{\parallel}) e^{i\mathbf{k}'_{\parallel} \cdot \mathbf{r}_{\parallel}} \mathrm{d}\mathbf{k}'_{\parallel}, \tag{S5}$$

where $\mathbf{k} = (\mathbf{k}_{\parallel}, \gamma)$ is the wave vector in the object space, with $\mathbf{k}_{\parallel} = (k_{\text{x}}, k_{\text{y}})$ and $\gamma = \sqrt{n^2 k_0^2 - k_{\parallel}^2}$, while $\mathbf{k}' = (\mathbf{k}'_{\parallel}, \gamma')$ is the wave vector in the image space, with $\mathbf{k}'_{\parallel} = \mathbf{k}_{\parallel}/M$ and $\gamma' = \sqrt{k_0^2 - k_{\parallel}'^2}$. The integration of $\mathbf{k}$ operates at $|\mathbf{k}|$ constant and over the numerical aperture of the objective. The function $h(M\mathbf{k}'_{\parallel})$ is a cutoff function taking into account the numerical aperture of the objective lens. $\mathbf{e}'(M\mathbf{k}'_{\parallel})$ is a vectorial function proportional to the field radiated by the dipole $\mathbf{p}$ in the Fourier space of the microscope. It reads[**?**]

$$\mathbf{e}'(\mathbf{k}_{\parallel}) = \mathbb{R}(\mathbf{k}_{\parallel}) \mathbf{e}(\mathbf{k}_{\parallel}), \tag{S6}$$

where $\mathbb{R}$ is a rotation matrix and $\mathbf{e}(\mathbf{k}_\parallel)$ reads

$$\mathbf{e}(\mathbf{k}_\parallel) = \frac{ik_0^2}{8\varepsilon_0\pi^2}\frac{1}{\gamma}\left[\mathbf{p}-(\hat{\mathbf{k}}\cdot\mathbf{p})\hat{\mathbf{k}}\right]e^{-i\,nk_0\cdot(\mathbf{r}_0-\mathbf{r}_{ob})} \tag{S7}$$

$$\mathbf{e}(\mathbf{k}_\parallel) = \frac{ik_0^2}{8\varepsilon_0\pi^2}\frac{1}{\gamma}\left[\mathbf{p}-(\hat{\mathbf{k}}\cdot\mathbf{p})\hat{\mathbf{k}}\right]e^{i\,nk_0z_{ob}}, \tag{S8}$$

where $\hat{\mathbf{k}} = \mathbf{k}/(nk_0)$. By using Eqs Eq. (S4) and Eq. (S5), one can calculate the normalized complex transmission coefficient of the system defined as

$$\frac{t}{t_0}(\mathbf{r}_\parallel) = \frac{\mathbf{E}_{tot,im}(\mathbf{r}_\parallel)\cdot\mathbf{E}^\star_{ex,im}}{|\mathbf{E}_{ex,im}|^2}. \tag{S9}$$

Since

$$\mathbf{E}_{tot,im}(\mathbf{r}_\parallel) = \mathbf{E}_{ex,im} + M\iint_{N.A.}\sqrt{\frac{\gamma}{\gamma'}}h(M\mathbf{k}'_\parallel)\mathbf{e}'(M\mathbf{k}'_\parallel)e^{i\mathbf{k}'_\parallel\cdot\mathbf{r}_\parallel}\mathrm{d}\mathbf{k}'_\parallel, \tag{S10}$$

one has

$$\frac{t}{t_0}\left(\mathbf{r}_\parallel\right) = 1+\frac{M^3}{nE_0^2}\iint_{N.A.}\sqrt{\frac{\gamma}{\gamma'}}h(M\mathbf{k}'_\parallel)\mathbf{e}'(M\mathbf{k}'_\parallel)\cdot\mathbf{E}^\star_{ex,im}\,e^{i\mathbf{k}'_\parallel\cdot\mathbf{r}_\parallel}\mathrm{d}\mathbf{k}'_\parallel \tag{S11}$$

$$\iint_{image}\left(\frac{t}{t_0}\left(\mathbf{r}_\parallel\right)-1\right)d\mathbf{r}_\parallel = \frac{M^3}{nE_0^2}\iint_{image}\iint_{N.A.}\sqrt{\frac{\gamma}{\gamma'}}h(M\mathbf{k}'_\parallel)\mathbf{e}'(M\mathbf{k}'_\parallel)\cdot\mathbf{E}^\star_{ex,im}\,e^{i\mathbf{k}'_\parallel\cdot\mathbf{r}_\parallel}\mathrm{d}\mathbf{k}'_\parallel\mathrm{d}\mathbf{r}_\parallel \tag{S12}$$

$$\iint_{image}\left(\frac{t}{t_0}\left(\mathbf{r}_\parallel\right)-1\right)d\mathbf{r}_\parallel = \frac{M^3}{nE_0^2}\iint_{N.A.}\sqrt{\frac{\gamma}{\gamma'}}h(M\mathbf{k}'_\parallel)\mathbf{e}'(M\mathbf{k}'_\parallel)\cdot\mathbf{E}^\star_{ex,im}\,d\mathbf{k}'_\parallel\iint_{image}e^{i\mathbf{k}'_\parallel\cdot\mathbf{r}_\parallel}\mathrm{d}\mathbf{r}_\parallel. \tag{S13}$$

Giving

$$\iint_{image}e^{i\mathbf{k}'_\parallel\cdot\mathbf{r}_\parallel}\mathrm{d}\mathbf{r}_\parallel = 4\pi^2\delta(\mathbf{k}'_\parallel), \tag{S14}$$

where δ is the Dirac function, Eq. (S13) becomes

$$\iint_{image}\left(\frac{t}{t_0}\left(\mathbf{r}_\parallel\right)-1\right)d\mathbf{r}_\parallel = \frac{M^3}{nE_0^2}4\pi^2\sqrt{\frac{\gamma(0)}{\gamma'(0)}}h(0)\mathbf{e}'(0)\cdot\mathbf{E}^\star_{ex,im} \tag{S15}$$

where

$$\mathbf{e}'(0) = \mathbb{R}(0)\mathbf{e}(0) = \frac{ik_0^2}{8\pi^2\varepsilon_0}\frac{1}{\gamma(0)}\mathbb{I}\left[\mathbf{p}-(\hat{\mathbf{k}_0}\cdot\mathbf{p})\hat{\mathbf{k}_0}\right]e^{ink_0z_{ob}}, \tag{S16}$$

$$\gamma(0) = nk_0, \tag{S17}$$

$$\gamma'(0) = k_0, \tag{S18}$$

$$h(0) = 1, \tag{S19}$$

$$\mathbf{E}_{ex,im} = \frac{\sqrt{n}}{M}\mathbf{E}_0e^{ink_0z_{ob}} = \frac{\sqrt{n}}{M}\mathbf{E}_{ex,ob}e^{ink_0z_{ob}} \tag{S20}$$

And since $\mathbf{k}_0\cdot\mathbf{E}^\star_{ex,im} = 0$ and giving the definition of α (Eq. Eq. (S1)), one gets

$$\iint_{image}\left(\frac{t}{t_0}\left(\mathbf{r}_\parallel\right)-1\right)\mathrm{d}\mathbf{r}_\parallel = \frac{ik_0M^2}{2n}\alpha. \tag{S21}$$

The integration runs over the image plane, i.e., over the space of camera sensor $\mathbf{r}_\parallel = (x_{im}, y_{im})$. By changing the $\mathbf{r}_\parallel$ variable into the variables x, y running over the object plane, the factor M^2 simplifies: $\mathrm{d}\mathbf{r}_\parallel = \mathrm{d}x_{im}\mathrm{d}y_{im} = M^2\mathrm{d}x\mathrm{d}y$. One gets this way the final expression of the polarizability

$$\boxed{\alpha = \frac{i\lambda_0 n}{\pi}\iint_{image}\left(1-\frac{t}{t_0}(x,y)\right)\mathrm{d}x\mathrm{d}y}, \tag{S22}$$

where $\frac{t}{t_0}(x,y) = \sqrt{T(x,y)}e^{i\frac{2\pi}{\lambda_0}\delta\ell(x,y)}$ with $T(x,y)$ and $\delta\ell(x,y)$ are the measured transmission and OPD images.

B. Independence of the focus

From Eqs. Eq. (S15) and Eq. (S20), one can see that z_{ob} simplifies and does not affect the final expression of the polarizability. This shows that the position of the dipole along z, i.e., the focus of the microscope does not affect the measurements of the polarizability.

The interpretation of this effect is the following. The procedure is based on a pixel summation. Summing the pixels of an image amounts to extract the zero spatial frequency of an image. And the zero spatial frequency only arises from the wave vector aligned with the optical axis. Off-axis wave vectors only endow the image with spatial information (sine waves) that will be cancelled by pixel summation. This is why reducing the numerical aperture, which only affects these off-axis wave vectors, does not affect the measurements.

C. Independence of the numerical aperture of collection

Eq. Eq. (S14) indicates that only the forward wave vector along $\mathbf{k}_0$ contains the information. Wave vector $\mathbf{k}_{\parallel} \neq 0$ are cancelled out by the integration, i.e., by the pixel summation. Consequently, modifying the numerical aperture of the objective lens of the microscope does not change the measured value of α using Eq. (S22).

D. Generalization to extended particles

Let us consider now a particle occupying a domain $\mathcal{V}$ which radiates light through a polarization density field $\mathbf{P}(\mathbf{r})$, $\mathbf{r} \in \mathcal{V}$. In this case, Eq. Eq. (S8), defined for a dipole, now becomes

$$\mathbf{e}(\mathbf{k}_{\parallel}) = \frac{ik_0^2}{8\varepsilon_0\pi^2} \iiint_{\mathcal{V}} \frac{1}{\gamma} \left[\mathbf{P}(\mathbf{r}) - (\hat{\mathbf{k}} \cdot \mathbf{P}(\mathbf{r}))\hat{\mathbf{k}}\right] e^{-i\,n\mathbf{k}_0\cdot(\mathbf{r}-\mathbf{r}_{ob})} \mathrm{d}\mathbf{r}. \tag{S23}$$

One can then use this expression and conduct the same derivation as from Eq. Eq. (S8) to Eq. Eq. (S15). Then, Eq. Eq. (S16) becomes

$$\mathbf{e}'(0) = \mathbb{R}(0)\mathbf{e}(0) = \frac{ik_0^2}{8\pi^2\varepsilon_0} \frac{1}{\gamma(0)} \mathbb{I} \iiint_{\mathcal{V}} \left[\mathbf{P}(\mathbf{r}) - (\hat{\mathbf{k}_0} \cdot \mathbf{P}(\mathbf{r}))\hat{\mathbf{k}_0}\right] e^{-in\mathbf{k}_0\cdot(\mathbf{r}-\mathbf{r}_{ob})} \mathrm{d}\mathbf{r}, \tag{S24}$$

which then gives the same Eq.Eq. (S21) if one considers this definition

$$\alpha = \frac{1}{\varepsilon_0 |\mathbf{E}_0|^2} \iiint_{\mathcal{V}} \mathbf{E}^{\star}_{ex,ob}(\mathbf{r}) \cdot \mathbf{P}(\mathbf{r}) \mathrm{d}\mathbf{r}, \tag{S25}$$

which is how we define the generalized polarizability in the manuscript.

3. DETERMINATION OF THE EXTINCTION CROSS SECTION OF AN ARBITRARY OBJECT FROM THE OPTICAL THEOREM

Most of the quantities we use in this section are defined in the first section of this document.

The optical theorem states that the extinction cross section of any object can be determined from the sole knowledge of the complex scattered field in the forward direction. It is written as [7]:

$$\sigma_{ext} = \frac{4\pi}{k} \mathrm{Im}\left[\mathbf{E}_0^{\star} \cdot \mathbf{S}(\hat{\mathbf{k}}_{inc})\mathbf{E}_0\right] / |\mathbf{E}_0|^2 \tag{S26}$$

where $\mathbf{S}(\hat{\mathbf{k}}_{inc})$ is the scattering matrix, $k = nk_0$ and $\hat{\mathbf{k}}_{inc}$ is the unit vector in the incidence direction.

In our case, the measurements are done using an optical microscope, thus, we express σ_{ext} as a function of the quantities at the image plane of the microscope as follows

$$\sigma_{ext} = \frac{4\pi}{k} \mathrm{Im}\left[\mathbf{E}^{\star}_{ex,im} \cdot \mathbf{S}_{im}(\hat{\mathbf{k}}_{inc})\mathbf{E}_{ex,im}\right] / |\mathbf{E}_{ex,im}|^2, \tag{S27}$$

where $\mathbf{E}_{ex,im}$ is the excitation field at the image plane, it is given in Eq. Eq. (S4). $\mathbf{S}_{im}(\hat{\mathbf{k}})$ is linked to the scattered electric field at the image plane by:

$$\mathbf{E}_{s,im}\left(\mathbf{r}_{\parallel}\right) = \mathbf{S}_{im}(\hat{\mathbf{k}})\mathbf{E}_{ex,im} \frac{e^{ik_0 r}}{r}. \tag{S28}$$

However, as demonstrated in our previous work [**?**], $\mathbf{E}_{s,im}\left(\mathbf{r}_{\parallel}\right)$ can be expressed by a sum of plane waves as follows

$$\mathbf{E}_{s,im}\left(\mathbf{r}_{\parallel}\right) = M \iint \sqrt{\frac{\gamma}{\gamma'}} h(M\mathbf{k}'_{\parallel}) \mathbf{e}'(M\mathbf{k}'_{\parallel}) e^{i\mathbf{k}'_{\parallel}\cdot\mathbf{r}_{\parallel}} \mathrm{d}\mathbf{k}'_{\parallel}, \tag{S29}$$

where $\mathbf{e}'(M\mathbf{k}'_{\parallel})$ is a vectorial function proportional to the field radiated by the object in the Fourier space of the microscope (see ref [**?**] for more details)

The stationary phase theorem [8] states that any function written as a sum of plane waves as follows

$$\mathbf{E}\left(\mathbf{r}_{\parallel}, z\right) = \iint \mathbf{e}(\mathbf{k}_{\parallel}) e^{i\mathbf{k}_{\parallel}\mathbf{r}_{\parallel} + i\gamma z} \mathrm{d}\mathbf{k}_{\parallel}, \tag{S30}$$

can be written, when $\mathbf{r} = \left(\mathbf{r}_{\parallel}, z\right)$ tends to infinity, as:

$$\mathbf{E}\left(\mathbf{r}_{\parallel}, z\right) = -2i\pi\gamma\mathbf{e}(\mathbf{k}_{\parallel})\frac{e^{ik_0 r}}{r}. \tag{S31}$$

The application of the above theorem on Eq. Eq. (S29) gives

$$\mathbf{E}_{\mathrm{s,im}}\left(\mathbf{r}_{\parallel}\right) = -2i\pi\sqrt{\frac{\gamma}{\gamma'}}\gamma\mathbf{e}'(M\mathbf{k}'_{\parallel})\frac{e^{ik_0 r}}{r}. \tag{S32}$$

By identification between Eq. Eq. (S28) and Eq. Eq. (S32), we deduce

$$\mathbf{S}_{\mathrm{im}}(\hat{\mathbf{k}})\mathbf{E}_{\mathrm{ex,im}} = -2i\pi\sqrt{\frac{\gamma}{\gamma'}}\gamma\mathbf{e}'(M\mathbf{k}'_{\parallel}). \tag{S33}$$

Now, one can replace Eq. Eq. (S33) into Eq. Eq. (S27), this latter becomes

$$\sigma_{\mathrm{ext}} = \frac{4\pi}{k}\mathrm{Im}\left[\mathbf{E}^{\star}_{\mathrm{ex,im}} \cdot \left(-2i\pi\sqrt{\frac{\gamma_{\mathrm{inc}}}{\gamma'_{\mathrm{inc}}}}\gamma_{\mathrm{inc}}\mathbf{e}'(M\mathbf{k}'_{\parallel_{\mathrm{inc}}})\right)\right] / |\mathbf{E}_{\mathrm{ex,im}}|^2. \tag{S34}$$

Since in our experiments, we work at normal incidence $\mathbf{k}_{\mathrm{inc}} = (\mathbf{k}'_{\parallel_{\mathrm{inc}}}, \gamma_{\mathrm{inc}}) = (0, k)$ thus $\mathbf{e}'(M\mathbf{k}'_{\parallel_{\mathrm{inc}}}) = \mathbf{e}'(0)$. By doing a Fourier transform for Eq. Eq. (S5), we can determine $\mathbf{e}'(0)$ as a function of the scattered electric field at the image plane $\mathbf{E}_{\mathrm{s,im}}$, it is given by

$$\mathbf{e}'(0) = \frac{1}{4\pi^2\sqrt{n}}\iint \mathbf{E}_{\mathrm{s,im}}\left(\mathbf{r}_{\parallel}\right) d\mathbf{r}_{\parallel} = \frac{1}{4\pi^2\sqrt{n}}\iint \left(\mathbf{E}_{\mathrm{tot,im}} - \mathbf{E}_{\mathrm{ex,im}}\right) \mathrm{d}\mathbf{r}_{\parallel}, \tag{S35}$$

where $\mathbf{E}_{\mathrm{tot,im}} = \mathbf{E}_{\mathrm{ex,im}} + \mathbf{E}_{\mathrm{s,im}}$ is the total electric field at the image plane. By introducing Eq. Eq. (S16) in Eq. Eq. (S34), we can express the extinction cross section as a function of the normalized complex transmission coefficient defined as $\frac{t}{t_0} = \frac{\mathbf{E}_{\mathrm{tot,im}} \cdot \mathbf{E}^{\star}_{\mathrm{ex,im}}}{|\mathbf{E}_{\mathrm{ex,im}}|^2}$, it reads

$$\sigma_{\mathrm{ext}} = 2\mathrm{Re}\left[\iint_{\mathrm{image}}\left(1 - \frac{t}{t_0}(x,y)\right)\mathrm{d}x\mathrm{d}y\right], \tag{S36}$$

where $\frac{t}{t_0}(x,y) = \sqrt{T(x,y)}e^{i\frac{2\pi}{\lambda_0}\delta\ell(x,y)}$ with $T(x,y)$ and $\delta\ell(x,y)$ are the measured transmission and OPD images.

4. SEM IMAGES OF POLYSTYRENE AND GOLD NANOPARTICLES

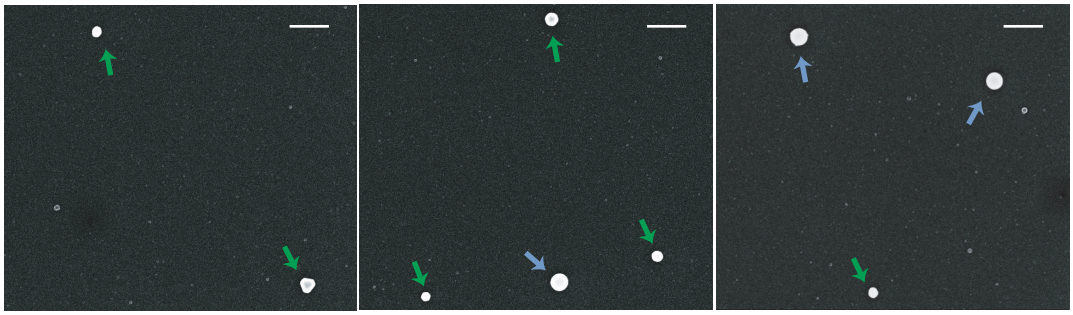

Fig. S4. Examples of the SEM images of gold and polystyrene nanoparticles showing the dispersion in size and shape. Gold nanoparticles ($d \sim 100$ nm) are indicated with green arrows and polystyrene ($d \sim 200$ nm) with blue arrows. Scale bar is 500 nm.

5. DISPERSION OF THE MEASUREMENTS

Figure S5 displays measurements of nanoparticle polarizabilities correlation with their size measured by SEM. A clear correlation exists, indicating that the main origin of the dispersion of the measurements is the size dispersion of the nanoparticles.

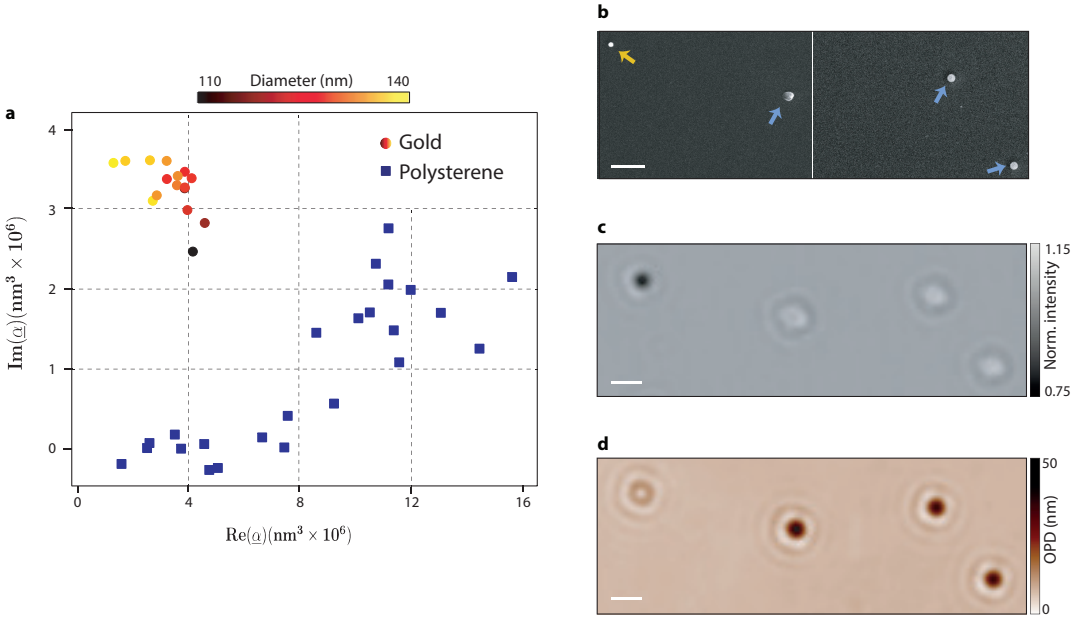

Fig. S5. Influence of the particle size on the optical polarizabilities of gold and polystyrene nanospheres. The particles were dispersed on the same glass substrate, in air. (a) Polarizabilities values plotted in the complex plane. (c) SEM image of gold (orange arrow) and polystyrene (blue arrows) nanoparticules. (d) Normalized intensity and (e) OPD images of the same area as (c).

6. ERROR BARS

The error bars in Figure 2b,f were not displayedin the main manuscript for the sake of readability. They are displayed here in Figure S6.

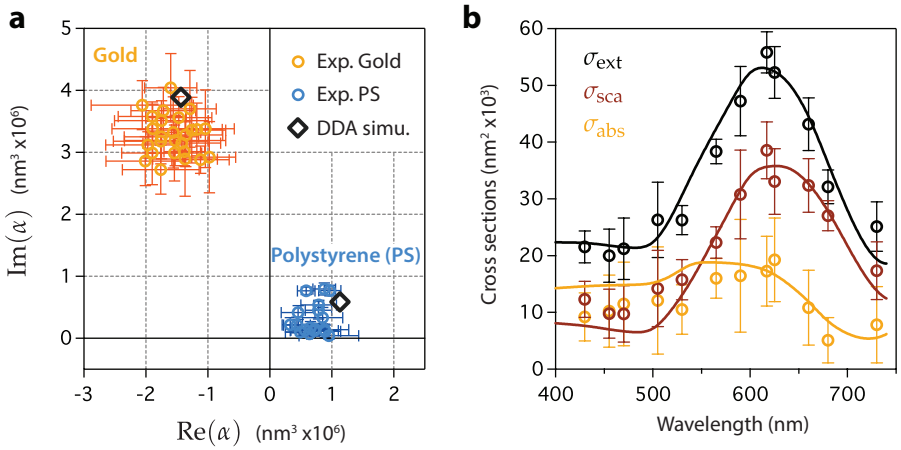

Fig. S6. Influence of the particle size on the optical polarizabilities of gold and polystyrene nanospheres. The particles were dispersed on the same glass substrate, in air. (a) Polarizabilities values plotted in the complex plane. (c) SEM image of gold (orange arrow) and polystyrene (blue arrows) nanoparticules. (d) Normalized intensity and (e) OPD images of the same area as (c).

7. FABRICATION PROCESS OF GOLD NANORODS AND SEM IMAGES

Fabrication of samples. Glass microscope slides (No 1.5) are consecutively washed in isopropanol and acetone under sonication for five minutes, respectively. Hereafter, a plasma etching step is performed (O_2 at 50 W and 250 mTorr for 30 s) to rid the surface of possible organic contamination. A layer of resist (PMMA AC MCC NANO 950k A4) is spin-coated at 3000 rpm to a thickness of 240 nm, and subsequently baked in a convection oven at 180°C for 10 min. The surface is hereafter rendered hydrophilic through a plasma etching step (O_2 at 50 W and 250 mTorr for 5 s). A solution of PDDA in water (0.2 %) is put on the sample for 30 s and subsequently rinsed in deionized water for 20 s. At this point polystyrene bead (80 nm microparticles Gmbh, Germany) are diluted in water to a concentration of 2.5 ppm. The PS bead solution is drop-casted on the PDDA functionalized substrates for 20 s and hereafter rinsed in water for 30 s. At this point a 10 nm Au mask is deposited at normal incidence, followed by PS beads removal through tape stripping. To expose the underlying glass substrate and produce a sufficient resist undercut, dry etching (O_2 at 50 W and 250 mTorr for 7 min) is performed. The final nanorods are formed by evaporating Au at a rate of 0.2 nm/s as the mounting stage was continuously tilting between positive and negative angles (maximum of 10°, determining the aspect ratio of the nanorods) repetitively 7 times. Hereafter, a lift-off procedure is performed in acetone and followed by annealing at 150°C on a hotplate for 10 minutes to improve crystallinity and optical properties of the nanorods.

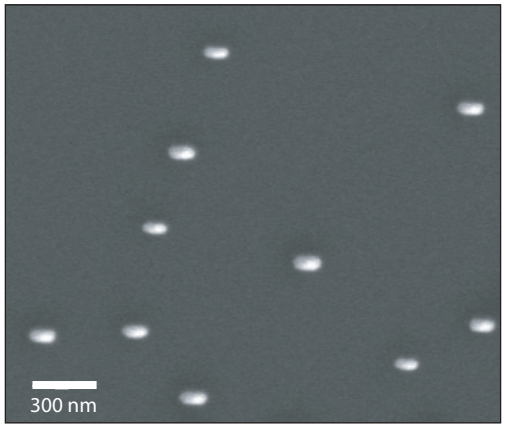

Fig. S7. Examples of the SEM image of gold nanorods showing the dispersion in size and aspect ratios.

REFERENCES

1. P. Bon, G. Maucort, B. Wattellier, and S. Monneret, "Quadriwave lateral shearing interferometry for quantitative phase microscopy of living cells," Opt Express **17**, 13080–94 (2009).
2. G. Baffou, P. Bon, J. Savatier, J. Polleux, M. Zhu, M. Merlin, H. Rigneault, and S. Monneret, "Thermal imaging of nanostructures by quantitative optical phase analysis," Acs Nano **6**, 2452–2458 (2012).
3. S. Khadir, P. Bon, D. Vignaud, E. Galopin, N. McEvoy, D. McCloskey, S. Monneret, and G. Baffou, "Optical imaging and characterization of graphene and other 2d materials using quantitative phase microscopy," ACS Photonics **4**, 3130–3139 (2017).
4. J. Primot and N. Guérineau, "Extended hartmann test based on the pseudoguiding property of a hartmann mask completed by a phase chessboard," Appl. Opt. **39**, 5715–5720 (2000).
5. P. Bon, S. Monneret, and B. Wattellier, "Noniterative boundary-artifact-free wavefront reconstruction from its derivatives," Appl. Opt. **51**, 5698–5704 (2012).
6. P. Bon, S. Aknoun, S. Monneret, and B. Wattellier, "Enhanced 3d spatial resolution in quantitative phase microscopy using spatially incoherent illumination," Opt. Express **22**, 8654–8671 (2014).
7. M. J. Berg, C. M. Sorensen, and A. Chakrabarti, "Extinction and the optical theorem. part i. single particles," J. Opt. Soc. Am. A **25**, 1504–1513 (2008).
8. M. Born and E. Wolf, *Principles of Optics: Electromagnetic Theory of Propagation, Interference and Diffraction of Light* (Cambridge University Press, 1999).